Chinese Chemical Letters 37 (2026) 110709

Contents lists available at ScienceDirect

Chinese Chemical Letters

journal homepage: www.elsevier.com/locate/cclet

Ion exchange for enhancing MOF adsorbents performance in humid C_2H_2/CO_2 separation

Muzi Li, Xin Zhang, Xiang-Jing Kong, Qiancheng Chen, Xuefeng Bai, Tao He*, Jian-Rong Li

Beijing Key Laboratory for Green Catalysis and Separation and Department of Chemical Engineering, College of Materials Science and Engineering, Beijing University of Technology, Beijing 100124, China

ARTICLE INFO

Article history:
Received 1 October 2024
Revised 22 November 2024
Accepted 3 December 2024
Available online 4 December 2024

Keywords:
Metal-organic framework
Ion exchange
Acetylene purification
C_2H_2/CO_2 separation
Humid condition

ABSTRACT

The gas separation performance of metal-organic framework (MOF) adsorbents could be enhanced by tuning the pores, whereas the presence of moisture usually compromises the efficiency. Herein, two MOFs, Fe-BDC-TPT-BF_4, Ni-BDC-TPT-TMA ($TMA^+ = (CH_3)_4N^+$), were synthesized by exchanging countering ions in parent MOFs, Fe-BDC-TPT-Cl and Ni-BDC-TPT-Me_2NH_2, respectively. Fe-BDC-TPT-BF_4 and Ni-BDC-TPT-TMA exhibited a high C_2H_2 adsorption uptake of 203.1 cm^3/g and 200.1 cm^3/g at 298 K and 1 bar, and high C_2H_2/CO_2 selectivity of 4.6 and 4.4. Humid breakthrough experiments revealed that high C_2H_2 productivity of high C_2H_2 purity was achieved on Ni-BDC-TPT-TMA at 35% relative humidity. Cycling dynamic breakthrough experiments demonstrate good recyclability of Ni-BDC-TPT-TMA for humid C_2H_2/CO_2 separation. The alteration of countering ions changed the pore size and chemistry, leading to high C_2H_2 uptake, high C_2H_2 selectivity, and retained performance in the presence of moisture, making it a promising candidate for practical applications. This work highlights that ion exchange modification of MOFs has been developed as a facile and powerful strategy to optimize the inner pores for better performance in challenging separations.

© 2025 Published by Elsevier B.V. on behalf of Chinese Chemical Society and Institute of Materia Medica, Chinese Academy of Medical Sciences.

Acetylene (C_2H_2) is a crucial feedstock in the chemical industry, extensively utilized in the production of various commercial chemicals, including vinyl chloride, acrylic acid, and 1,4-butynediol [1]. Typically, C_2H_2 is generated through the combustion of natural gas or the thermal cracking of hydrocarbons [1,2]. In these processes a significant amount of carbon dioxide (CO_2) also forms as a byproduct [3]. Moreover, due to the use of water for quenching, raw C_2H_2 products also contain humidity. It is highly desired to develop efficient C_2H_2 purification techniques to meet the demand across different sectors. However, separating C_2H_2 from CO_2 presents a challenge due to their nearly identical molecular size (kinetic diameter of 3.3 Å for both) and shape, as well as similar physical properties (Table S1 in Supporting information) [4–9]. Traditional purification methods, including solvent extraction and cryogenic distillation [10], are both energy-intensive and inefficient. Therefore, adsorptive separation based on porous physisorbents has aroused broad interest thanks to the merits of low energy footprint and purpose-oriented material design.

By virtue of great structure diversity and structure tunability, metal-organic frameworks (MOFs) have been developed as a promising community of porous physisorbents for adsorptive gas separation [11–17]. The modular nature enables MOFs to be tailored for achieving molecular sieving (pore size tuning) or enhancing separation performance (pore environment/chemistry tuning, such as incorporating specific binding sites) [18–21]. The introduction of functional groups through ligand design to construct hydrophobic pores in MOFs has been proven to be an effective method for improving the stability of MOFs, and meanwhile improving their separation ability of C_2H_2/CO_2 [22–24], C_2H_6/C_2H_4 [25–28], C_3H_8/C_3H_6 [29], *n*-C_4H_{10}/*iso*-C_4H_{10} [30] and CO_2/N_2 [31,32] under humid conditions. In addition, ionic MOFs offer unique advantages for gas adsorption and separation due to their amenability to ion exchange [33–35]. The variation of cationic or anionic species within the pores allows for facile modification of the pore chemistry, which can significantly alter their capacity and selectivity in gas adsorption [33]. Exchanging the ions in MOFs can open up new opportunities to develop advanced physisorbents potentially addressing challenges in important separations. Herein, we synthesized two new ionic MOFs, Fe-BDC-TPT-BF_4, Ni-BDC-TPT-TMA ($TMA = (CH_3)_4N^+$), from their parent frameworks Fe-BDC-TPT-Cl and Ni-BDC-TPT-Me_2NH_2, respectively (Fig. 1), through ion exchange. To evaluate the effect of counter ions on gas separation performance of the resulting MOFs, static single-component gas adsorption experiments (C_2H_2 and CO_2) and dynamic breakthrough

* Corresponding author.
E-mail address: hetao@bjut.edu.cn (T. He).

https://doi.org/10.1016/j.cclet.2024.110709
1001-8417/© 2025 Published by Elsevier B.V. on behalf of Chinese Chemical Society and Institute of Materia Medica, Chinese Academy of Medical Sciences.

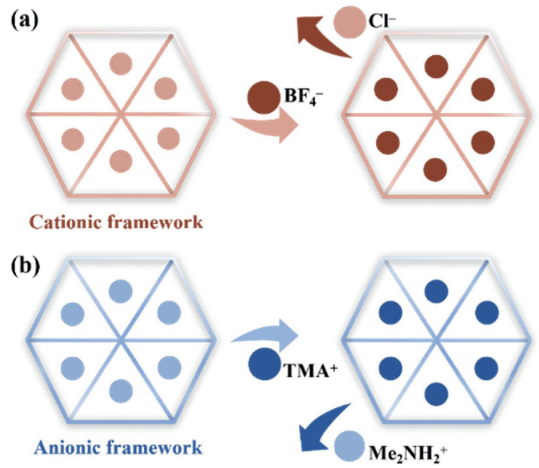


Fig. 1. Anion and cation exchange strategy: (a) Exchange Cl^- in Fe-BDC-TPT-Cl with BF_4^-. (b) Exchange $Me_2NH_2^+$ in Ni-BDC-TPT-Me_2NH_2 with TMA^+.

experiments (C_2H_2/CO_2 separation under dry/wet conditions) were performed on Fe-BDC-TPT-BF_4 and Ni-BDC-TPT-TMA, and compared with their parent MOFs.

The Fe/Ni-BDC-TPT-X (X = Cl, Me_2NH_2) series exhibits a good confinement effect due to the implementation of the pore space partition strategy, which effectively enhances the interaction between the framework and gas molecules, as demonstrated in the separation of $C_2H_2/C_2H_4/C_2H_6$ [35], C_2H_2/CO_2 [36–38]. Specifically, Fe-BDC-TPT-Cl made with Fe incorporates anionic counterions, while those made with Ni incorporate cationic counterions. This difference in counterion incorporation influences the framework's interaction with specific gas molecules, making these materials highly effective for various gas separation applications. Therefore, Fe/Ni-BDC-TPT-X can modulate pore size and chemistry through ion exchange strategies, making it an excellent platform for post-synthesis modifications aimed at improving gas separation.

Fe-BDC-TPT-Cl and Ni-BDC-TPT-Me_2NH_2 were synthesized according to the literature [35]. Subsequently, Fe-BDC-TPT-BF_4, and Ni-BDC-TPT-TMA were prepared by ion exchange with Fe-BDC-TPT-Cl and Ni-BDC-TPT-Me_2NH_2, respectively (Fig. 1). ^1H NMR confirmed that the exchange percentage for all samples exceeded 95% (Figs. S1 and S2, Tables S2-S5 in Supporting information). The phase purity of the samples was confirmed by comparing the powder X-ray diffraction (PXRD) patterns with the calculated ones, which were found to be consistent (Fig. S3 in Supporting information). The PXRD patterns of Fe-BDC-TPT-Cl, Fe-BDC-TPT-BF_4, Ni-BDC-TPT-Me_2NH_2, and Ni-BDC-TPT-TMA were subjected to indexing and refinement using the Le Bail method. Tables S6-S9 (Supporting information) presented both the initial and refined parameters, while Figs. S4-S7 (Supporting information) showed the differences between the experimental and fitted PXRD patterns. These results confirm that all materials adopt an isostructural framework.

The permanent porosity of the four materials was confirmed by N_2 adsorption at 77 K. The isotherms of Fe-BDC-TPT-Cl, Fe-BDC-TPT-BF_4, Ni-BDC-TPT-Me_2NH_2 and Ni-BDC-TPT-TMA show N_2 uptakes of 586.2, 448.4, 379.3 and 317.5 cm^3/g, respectively, at 1 atm, belonging to Type-I adsorption isotherms. The N_2 uptakes for all the frameworks decreased in the following order: Ni-BDC-TPT-Me_2NH_2 > Ni-BDC-TPT-TMA, Fe-BDC-TPT-Cl > Fe-BDC-TPT-BF_4 (Fig. S8 in Supporting information). This trend is expected to occur due to the increasing size of exchange ions occupying the pore space, which aligns with the following order: $TMA^+ > Me_2NH_2^+ > BF_4^- > Cl^-$ (Table S10 in Supporting information). The Brunauer-Emmett-Teller (BET) surface area of Fe-BDC-TPT-Cl, Fe-BDC-TPT-BF_4, Ni-BDC-TPT-Me_2NH_2 and Ni-BDC-TPT-TMA was calculated to be 1677.4, 1307.8, 1236.4, 959.2 m^2/g, respectively. As the size of counter ions decreases, the pore size of Ni-BDC-TPT-TMA, Ni-BDC-TPT-Me_2NH_2, Fe-BDC-TPT-BF_4 and Fe-BDC-TPT-Cl increase sequentially, as follows: 4.7, 6.5, 6.7, 8.6 Å (Fig. S9 in Supporting information). The chemical stability of them was tested by soaking in water for 24 h. The crystallinity of these materials remained preserved (Fig. S3). After water treatment, the N_2 adsorption capacities of Fe-BDC-TPT-BF_4 and Ni-BDC-TPT-TMA decreased to 269.2 and 266.5 cm^3/g, respectively, showing reductions of 179.2 and 51.0 cm^3/g (Fig. S10 in Supporting information). These results indicate that water has a smaller impact on Ni-BDC-TPT-TMA.

To investigate the adsorption performance of various materials for C_2H_2 and CO_2 both before and after ion exchange, as well as the separation performance of C_2H_2/CO_2, the adsorption isotherms of four materials were performed at different temperatures and 1 bar. For the cationic framework, Fe-BDC-TPT-BF_4 exhibited enhanced gas adsorption capacity after ion exchange. Specifically, Fe-BDC-TPT-BF_4 demonstrated a C_2H_2 adsorption capacity of 203.1 cm^3/g and CO_2 adsorption capacity of 93.2 cm^3/g. In contrast, Fe-BDC-TPT-Cl only had a C_2H_2 adsorption capacity of 140.8 cm^3/g and a CO_2 adsorption capacity of 70.6 cm^3/g. Two anion frameworks also exhibited similar trends (Figs. 2a and b). Ni-BDC-TPT-Me_2NH_2 exhibited a C_2H_2 adsorption capacity of 166.0 cm^3/g and CO_2 adsorption capacity of 95.0 cm^3/g. The larger volume of TMA^+ increased the confinement effect, resulting in higher C_2H_2 adsorption capacity: 200.1 cm^3/g for Ni-BDC-TPT-TMA (Figs. 2c and d). The comparison of the adsorption capacity of CO_2 and C_2H_2 by the framework before and after ion exchange is shown in Fig. 2e. After ion exchange, the adsorption performance of the resulting material for both C_2H_2 and CO_2 changed to varying degrees. The narrow pore size and the formation of C–H···X (X = F, π) interaction with C_2H_2 may enhance the affinity between C_2H_2 molecule and framework, thereby significantly increasing the adsorption capacity of C_2H_2.

By studying the adsorption isotherms at 298 K and 273 K, and fitting the relevant data with the Virial equation, the isosteric adsorption heats (Q_{st}) of four materials were calculated. As shown in Figs. S11-S18 (Supporting information), the Q_{st} values for C_2H_2 are 40.7 and 55.3 kJ/mol for Fe-BDC-TPT-Cl and Fe-BDC-TPT-BF_4, respectively. For CO_2, the Q_{st} values are 9.4 and 28.2 kJ/mol, respectively. The higher Q_{st} for C_2H_2 compared to CO_2 in the cationic framework system indicates a stronger affinity of the framework for C_2H_2, consistent with the trend observed in the single-component adsorption curves. In the case of Ni-BDC-TPT analogs, Ni-BDC-TPT-TMA shows a significant increase in Q_{st} for C_2H_2 compared to Ni-BDC-TPT-Me_2NH_2. Specifically, the Q_{st} values for C_2H_2 are 24.3 kJ/mol and 31.2 kJ/mol for Ni-BDC-TPT-Me_2NH_2 and Ni-BDC-TPT-TMA, respectively. For CO_2, the Q_{st} values are 20.1 and 22.1 kJ/mol, respectively. The higher Q_{st} indicates that C_2H_2 molecules exhibit a stronger affinity for the framework, resulting in greater adsorption capacity. The larger difference in Q_{st} between C_2H_2 and CO_2 for Ni-BDC-TPT-TMA suggests a higher selectivity for C_2H_2 over CO_2. After ion exchange, the adsorption capacity for C_2H_2 in both Fe and Ni analogs increased, however, the corresponding Q_{st} did not show the same behavior (Fig. 2f).

The adsorption selectivity of the four materials for C_2H_2/CO_2 (50:50) was calculated using isothermal adsorption curve fitting parameters (Figs. S19-S24 and Tables S11-S14 in Supporting information) and ideal adsorption solution theory (IAST) at 298 K and 1 bar, respectively. The selectivity of Fe-BDC-TPT-BF_4 increases from 2.7 before ion exchange to 4.6 after exchange. Calculations show that the selectivity of the anion framework system for C_2H_2/CO_2 has also improved after ion exchange. The selectivity of Ni-BDC-TPT-Me_2NH_2 and Ni-BDC-TPT-TMA for C_2H_2/CO_2 is 2.5, 4.4, respectively. Different ion exchange percentages of Ni-BDC-TPT-TMA on

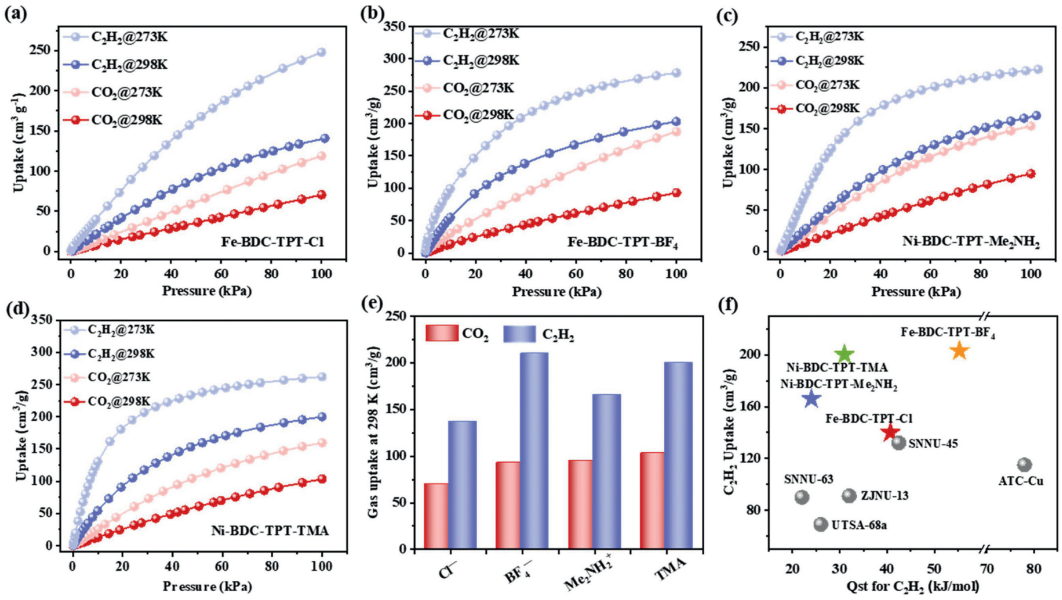


Fig. 2. C_2H_2 and CO_2 adsorption isotherms of (a) Fe-BDC-TPT-Cl, (b) Fe-BDC-TPT-BF_4, (c) Ni-BDC-TPT-Me_2NH_2 and (d) Ni-BDC-TPT-TMA at 298 K and 1 bar. (e) Comparison of adsorption capacity of four materials. (f) Comparison of C_2H_2 adsorption capacity and Q_{st} of various materials.

the adsorption isotherms were also tested. When the exchange percentage is 51.0% and 64.1%, the C_2H_2/CO_2 selectivity is 4.1 and 4.0, respectively (Figs. S25-S29 in Supporting information). These results indicate that optimal separation efficiency for C_2H_2/CO_2 can be achieved through complete exchange with TMA^+. Among them, the selectivity of Fe-BDC-TPT-BF_4 and Ni-BDC-TPT-TMA surpasses that of many other materials for C_2H_2/CO_2 separation, such as CAU-10-H (4.0) [39], UTSA-222 (4.0) [40], ZJNU-100 (3.8) [41], FJU-36a (2.8) [42], CoV-bdc-tpt (2.6) [43], FJU-112 (4.2) [44], SNNU-278 (4.3) [45], HKUST-1 (2.4) [46] etc. (Table S6 in Supporting information).

To further investigate the separation performance of Fe-BDC-TPT-Cl, Fe-BDC-TPT-BF_4, Ni-BDC-TPT-Me_2NH_2, Ni-BDC-TPT-TMA for C_2H_2/CO_2, dynamic breakthrough column experiments were conducted at 298 K using an equimolar C_2H_2/CO_2 (50/50, v/v) dry mixture with a flow rate of 2 mL/min. As shown in Figs. 3a and b, Fe-BDC-TPT-BF_4 and Ni-BDC-TPT-TMA demonstrate more efficient separation. Specifically, for Fe-BDC-TPT-BF_4, compared with the parent material Fe-BDC-TPT-Cl, the signal of CO_2 is detected faster and the capture yield is slightly improved. The breakthrough interval has increased by nearly 15 min with a separation productivity of 124.6 L/kg. Similarly, Ni-BDC-TPT-TMA also exhibits improved separation performance for C_2H_2/CO_2 compared to Ni-BDC-TPT-Me_2NH_2. The retention time of Ni-BDC-TPT-TMA for C_2H_2 is about 20 min longer than Ni-BDC-TPT-Me_2NH_2, and the separation productivity has increased from 101.0 L/kg to 130.8 L/kg (Fig. 3c). In terms of comprehensive C_2H_2 adsorption capacity and production, Ni-BDC-TPT-TMA exceeds most similar materials, such as ZJU-50a (85.2 L/kg) [47], BUT-316 (50.3 L/kg) [48], SIXSIF-dps-Cu (45.7 L/kg) [49], SIXSIF-3-Ni (58.4 L/kg) (Fig. 3d) [5].

In industrial production, cracking streams inevitably contain small amounts of water vapor, which may affect the separation performance of MOFs. The water vapor adsorption isotherms of several materials were first tested at room temperature. As shown in Figs. S30 and S31 (Supporting information), Fe-BDC-TPT-Cl exhibits high water adsorption at low pressure, in contrast, Fe-BDC-TPT-BF_4 did not show significant water uptake until the P/P_0 reached 0.2, indicating its lower affinity for water. The water uptake of Ni-BDC-TPT-Me_2NH_2 begins to increase sharply at lower pressures with a P/P_0 of 0.17, whereas Ni-BDC-TPT-TMA shows a sharp increase at a P/P_0 of 0.25. These results suggest that the materials became relatively more hydrophobic after ion exchange. To explore the separation ability of Fe-BDC-TPT-BF_4 and Ni-BDC-TPT-TMA under typical working conditions, breakthrough experiments were conducted in humid conditions. From the experimental results (Figs. 4a-c), it can be observed that under 35% RH, Fe-BDC-TPT-BF_4 shows that the breakthrough time for CO_2 remains nearly unchanged, while the breakthrough time for C_2H_2 significantly decreases (about 18 min). Despite showing slightly earlier breakthrough times for both CO_2 and C_2H_2 compared to dry feed gas conditions, Ni-BDC-TPT-TMA maintains its C_2H_2 purity and yield without significant decrease. The C_2H_2 adsorption capacity under humid conditions was calculated as 112.7 cm^3/g, which is 86.0% of the capacity for dry gas. And under 35% RH, Ni-BDC-TPT-TMA underwent five breakthrough cycles without a significant decline in separation performance (Fig. 4d). Desorption of Ni-BDC-TPT-TMA with He at a flow rate of 10 mL/min yielded a C_2H_2 desorption amount of 113.8 cm^3/g, aligning with the calculated value (Fig. S32 in Supporting information). Additionally, the PXRD pattern of Ni-BDC-TPT-TMA sample remained unchanged after the cyclic experiments (Fig. S33 in Supporting information), demonstrating its high durability during the C_2H_2/CO_2 separation process.

In summary, we have varied the countering ions in Fe-BDC-TPT-Cl and Ni-BDC-TPT-Me_2NH_2 through ion exchange to tune their gas separation properties. Altering $Me_2NH_2^+$ to TMA^+ significantly increases the density of methyl groups within the pores of Ni-BDC-TPT-TMA, leading to a high C_2H_2 adsorption capacity (200.1 cm^3/g at 298 K and 1 bar), along with a commendable C_2H_2/CO_2 selectivity (4.4 at 298 K and 1 bar). More importantly, this modification improves the hydrophobicity of the pores in Ni-BDC-TPT-TMA, exhibiting maintained C_2H_2/CO_2 separation performance and good recyclability in breakthrough experiments under 35% RH. This work has not only contributed new physisorbents through a facile synthesis and modification strategy, but also leveraged the material design principles for better structure functionalization and performance optimization. By tailoring the pores of MOFs, including adding, changing and removing specific entities, we can manipulate the physical and chemical properties of physisorbents to be equipped with more strengths, which are likely to help address the social and industrial challenges, even under harsh conditions.

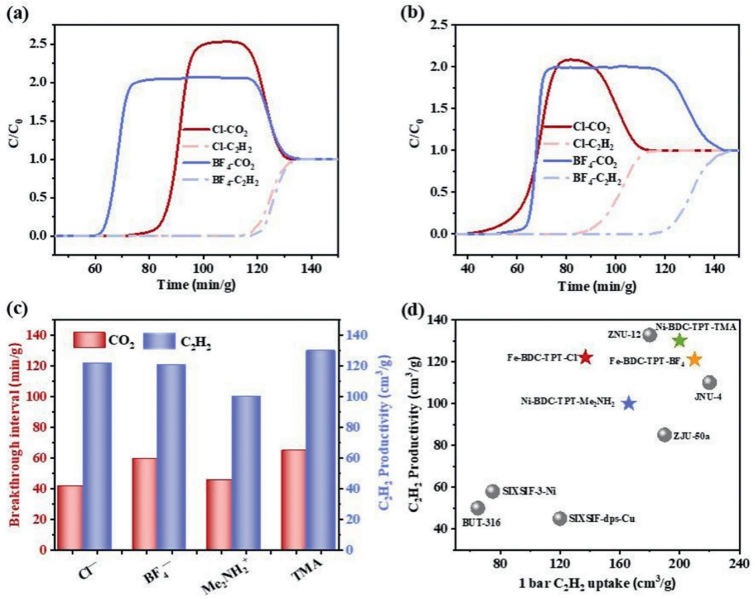


Fig. 3. The breakthrough curve of four materials for $V_{C_2H_2}:V_{CO_2} = 1:1$ with flow rate of 2 mL/min at 298 K, 1 bar: (a) Fe-BDC-TPT-Cl, Fe-BDC-TPT-BF_4; (b) Ni-BDC-TPT-Me_2NH_2, Ni-BDC-TPT-TMA. (c) Comparison of breakthrough interval and C_2H_2 productivity of four materials. (d) Comparison of C_2H_2 productivity and C_2H_2 adsorption capacity of different materials.

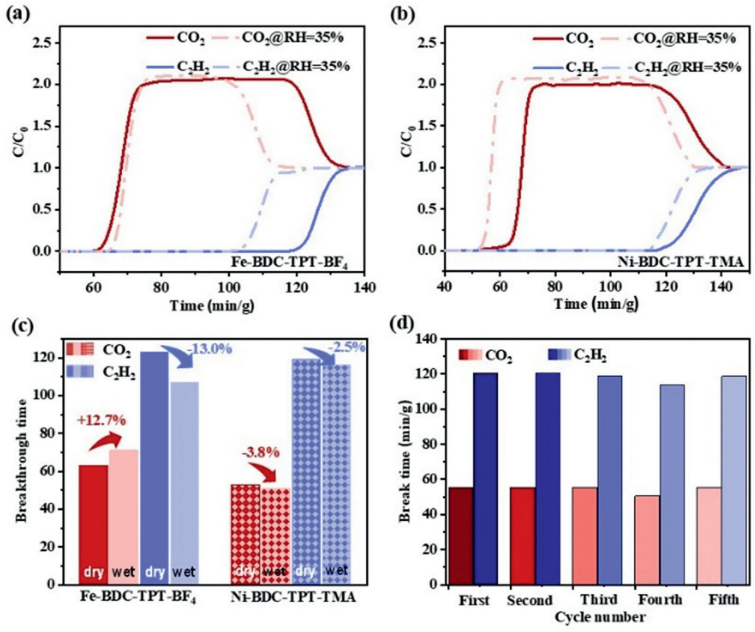


Fig. 4. Breakthrough curve of (a) Fe-BDC-TPT-BF_4, (b) Ni-BDC-TPT-TMA. (c) Comparison of Fe-BDC-TPT-BF_4 and Ni-BDC-TPT-TMA breakthrough time under dry and humid conditions. (d) Cycling experiments of C_2H_2/CO_2 (v/v = 1/1) separation for Ni-BDC-TPT-TMA.

Declaration of competing interest

The authors declare that they have no known competing financial interests or personal relationships that could have appeared to influence the work reported in this paper.

CRediT authorship contribution statement

Muzi Li: Writing – original draft, Investigation, Data curation. **Xin Zhang:** Writing – review & editing, Validation. **Xiang-Jing Kong:** Writing – review & editing, Data curation. **Qiancheng Chen:** Data curation. **Xuefeng Bai:** Software. **Tao He:** Writing – review & editing, Supervision, Funding acquisition. **Jian-Rong Li:** Writing – review & editing, Supervision, Project administration, Funding acquisition, Conceptualization.

Acknowledgments

We acknowledge the financial support from the National Natural Science Foundation of China (Nos. 22225803, 22038001, 22278011, 22108007 and 22401168) and the Beijing Natural Science Foundation (No. Z230023).

Supplementary materials

Supplementary material associated with this article can be found, in the online version, at doi:10.1016/j.cclet.2024.110709.

References

[1] H. Schobert, Chem. Rev. 114 (2014) 1743–1760.
[2] D.S. Sholl, R.P. Lively, Nature 532 (2016) 435–437.
[3] W. Fan, S. Yuan, W. Wang, et al., J. Am. Chem. Soc. 142 (2020) 8728–8737.
[4] R. Matsuda, R. Kitaura, S. Kitagawa, et al., Nature 436 (2005) 238–241.
[5] K.J. Chen, H.S. Scott, D.G. Madden, et al., Chem 1 (2016) 753–765.
[6] L. Yang, L. Yan, Y. Wang, et al., Angew. Chem. Int. Ed. 60 (2021) 4570–4574.
[7] S. Mukherjee, D. Sensharma, K.J. Chen, M.J. Zaworotko, Chem. Commun. 56 (2020) 10419–10441.
[8] L.Q. Yang, J. Yu, S.C. Fan, et al., J. Mater. Chem. A 12 (2024) 16427–16437.
[9] W. Li, J. Li, B. Zhang, et al., Chem. Eng. J. 483 (2024) 149126.
[10] G.T. Rochelle, Science 325 (2009) 1652–1654.
[11] H. Furukawa, K.E. Cordova, M. O'Keeffe, O.M. Yaghi, Science 341 (2013) 1230444.
[12] T. Islamoglu, Z. Chen, M.C. Wasson, et al., Chem. Rev. 120 (2020) 8130–8160.
[13] S.Q. Yang, T.L. Hu, Coord. Chem. Rev. 468 (2022) 214628.
[14] H. Daglar, H.C. Gulbalkan, G. Avci, et al., Angew. Chem. Int. Ed. 60 (2021) 7828–7837.
[15] W. Fan, X. Wang, B. Xu, et al., J. Mater. Chem. A 6 (2018) 24486–24495.
[16] Y.Y. Xue, J. Lei, H.J. Lv, et al., Small 20 (2024) e2311555.
[17] Y. Liang, G. Xie, K.K. Liu, et al., Angew. Chem. Int. Ed. 14 (2024) e202416884.
[18] P. Liu, J. Li, F. Yan, et al., Adv. Funct. Mater. 34 (2024) 2406664.
[19] H.Y. Li, X.J. Kong, S.D. Han, et al., Chem. Soc. Rev. 53 (2024) 5626–5676.
[20] J.R. Li, J. Yu, W. Lu, et al., Nat. Commun. 4 (2013) 1538.
[21] T. He, X.J. Kong, Z.X. Bian, et al., Nat. Mater. 21 (2022) 689–695.
[22] Y.L. Zhao, Q. Chen, X. Zhang, J.R. Li, Adv. Sci. 11 (2024) e2310025.
[23] W. Wang, W. Yuan, C. Kong, et al., J. Mater. Chem. A 11 (2023) 25605–25611.
[24] X.-J. Xie, H. Zeng, M. Xie, et al., Chem. Eng. J. 427 (2022) 132033.
[25] X.W. Gu, J. Pei, K. Shao, et al., ACS Appl. Mater. Interfaces 13 (2021) 18792–18799.
[26] X.J. Xie, Y. Wang, Q.Y. Cao, et al., Chem. Sci. 14 (2023) 11890–11895.
[27] H. Zeng, X.J. Xie, M. Xie, et al., J. Am. Chem. Soc. 141 (2019) 20390–20396.
[28] R. Wang, Q. Gao, Y.S. Zhong, et al., Sep. Purif. Technol. 304 (2023) 122332.
[29] Y. Wang, T. Li, L. Li, et al., Adv. Mater. 35 (2023) e2207955.
[30] L. Wang, W. Xue, H. Zhu, et al., Angew. Chem. Int. Ed. 62 (2023) e202218596.
[31] P.G. Boyd, A. Chidambaram, E. García-Díez, et al., Nature 576 (2019) 253–256.
[32] H. Zhu, W. Xue, H. Huang, et al., Sci. Bull. 68 (2023) 2531–2535.
[33] T. Wang, W. Mei, P. Li, et al., J. Mater. Chem. A 10 (2022) 22175–22181.
[34] C.N. Li, L. Liu, S. Liu, et al., Small 20 (2024) 2405561.
[35] M.Z. Li, X. Zhang, T. He, et al., Sep. Purif. Technol. 355 (2025) 129620.
[36] H. Yang, Y. Chen, C. Dang, et al., J. Am. Chem. Soc. 144 (2022) 20221–20226.
[37] F. Xiang, L. Li, Z. Yuan, et al., Chin. Chem. Lett. 36 (2025) 109672.
[38] K. Jiang, Y. Gao, P. Zhang, et al., Chin. Chem. Lett. 34 (2023) 108039.
[39] X. Zhang, R.B. Lin, H. Wu, et al., Chem. Eng. J. 431 (2022) 134184.
[40] J.X. Ma, J. Guo, H. Wang, et al., Inorg. Chem. 56 (2017) 7145–7150.
[41] Y. Wang, M. He, X. Gao, et al., Inorg. Chem. Front. 6 (2019) 263–270.
[42] X.B. Xu, Y. Yang, Z. Yuan, et al., Sep. Purif. Technol. 325 (2023) 124654.
[43] W. Wang, H. Yang, Y. Chen, et al., J. Am. Chem. Soc. 145 (2023) 17551–17556.
[44] F. Xiang, H. Zhang, Y. Yang, et al., Angew. Chem. Int. Ed. 62 (2023) e202300638.
[45] X. Mu, Y. Xue, M. Hu, et al., Chin. Chem. Lett. 34 (2023) 107296.
[46] M. Fischer, F. Hoffmann, M. Froba, ChemPhysChem 11 (2010) 2220–2229.
[47] K. Shao, H.M. Wen, C.C. Liang, et al., Angew. Chem. Int. Ed. 61 (2022) e202211523.
[48] X.Q. Wu, T. He, P.D. Zhang, et al., Chem. Eng. J. 482 (2024) 149115.
[49] J. Wang, Y. Zhang, Y. Su, et al., Nat. Commun. 13 (2022) 200.